# Effect of Camera Resolution on the Determination of Mechanical and Multiple Crack Properties of Engineered Cementitious Composites via Digital Image Correlation

**Eren Godek[1,2]** (ID) **Kamile Tosun Felekoglu[3]** (ID)

[1] Dokuz Eylul University, The Graduate School of Natural and Applied Science, Constr. Materials Program, Izmir, Türkiye

[2] Hitit University, Department of Construction Technology, Corum, Türkiye

[3] Dokuz Eylül University, Department of Civil Engineering, Izmir, Türkiye

*This article has been checked for similarity.*

---

**ABSTRACT**

In this study, the effect of image resolution on the determination of mechanical parameters and multiple crack properties of Engineered Cementitious Composites (ECC) was investigated by digital image correlation (DIC). For this purpose, low and high-resolution images were captured during the tensile loading of the ECC by using two cameras simultaneously. DIC analyses were performed on the images, and the results were compared both within themselves and with the traditional method. Mechanical parameters have been successfully calculated with DIC analysis and consistent values obtained with traditional methodology. However, the high-resolution images were found to be more effective for detecting pattern properties than the low-resolution images. It resulted in a low strain error when using the high-resolution images compared to the low-resolution images in DIC analysis. Finally, when the high-resolution images were used in DIC analysis as opposed to the low-resolution images, both the detected number of cracks and calculated crack widths were obtained accurately. This situation was proven by local strain maps provided by DIC.

**Keywords:**
ECC, DIC, Resolution, Tensile, Strain, Crack

## INTRODUCTION

Engineered Cementitious Composites (ECC) are advanced technology tailored cement-based composites that are well known today, with relatively higher strain capacity due to multiple cracking behaviors under tensile loading (1). Determination of basic mechanical parameters (stress, strain, and toughness i.e.) and understanding the multiple cracking behaviors of ECC are essential information for tailoring them from micro-scale designs to building constructions (2). Currently, traditional methods such as strain gauges and linear variable differential transformers (LVDT) are widely used for the determination of strain to investigate mechanical properties, and clip gauges to investigate crack properties. However, these methods have some drawbacks. Strain gauges may be susceptible to temperature and surface damage. LVDTs take readings, not directly from the surface of the samples and also within a limited length (3, 4). The use of clip gauges is effective for tracking the properties of pre-localized cracks or the region where the crack will occur can be predicted (5). On the other hand, it is ineffective for tracking the crack

properties of ECC due to the high number of random and unpredictable cracks.

Digital image correlation (DIC) is a non-contact surface tracking system based on images, a favored alternative to the aforementioned methods that can be used for both strain calculations and tracking crack propagation. The DIC method was introduced to the literature in the 1980s and was first used by Choi and Shah in 1997 to measure the deformation of concrete under compression (6-8).

The DIC system consists of a camera placed in front of the specimen and aligned directly to the surface. Images are taken at predetermined intervals during the mechanical tests. The DIC calculates the displacement vectors between a reference image taken from an undeformed surface at the beginning of the test and many images taken from a deforming surface during the loading. To make this calculation, a pattern called the speckle pattern should be applied to the surface of the specimen. This patterning process can be easily done

by generating random black dots on the pre-painted white surface. In the reference image, an area of interest (AOI) is determined, and this section is divided into a square group of pixels called subsets. Each subset includes a set of unique data owing to their speckle pattern, and the DIC tracks the movement of the subsets between the images by a defined pixel interval called the step size. By using a correlation algorithm, a displacement vector for the center point of each subset is calculated between the reference and deformed images, then converted to strain fields with strain formulations (9).

Various studies using the DIC method to monitor the mechanical performance and crack propagation of ECC are available in the literature. Horizontal deformations were measured with both DIC and LVDT in bending tests performed on beams produced using ECC. When the results were compared, it was determined that the obtained deformations gave consistent results (10). In another study by Ohno and Li (11), engineered polymeric fiber-reinforced geopolymer composites exhibiting multiple crack behavior under tensile stress were examined. In this study, it was shown that the composite reached crack saturation by detecting cracks larger than 20 microns in geopolymer composites with a 4-5% tensile strain capacity by the DIC method. Felekoğlu and Keskinateş (12) reported that the strain values obtained from both real and virtual LVDTs are close to each other and that the DIC method can be used to determine local deformations and deformation concentration regions. In addition, it has been shown that the number of cracks and crack width values at desired strain levels can be determined with the data obtained from DIC. Ding et al. (1) observed the failure behavior of steel-reinforced ECC beams and reinforced concrete beams with DIC and compared the formation and propagation of cracks by evaluating the entire loading process. In another recent study, DIC was used to monitor the deformation and crack formation of high-performance polyethylene fiber incorporating ECC specimens under bending and tensile loading (13). However, various factors affect the accuracy of strain calculations classified by Nwanoro et al. (14) as target image suitability, image quality, and DIC settings.

Image quality is one of the priority issues for the accuracy of the analysis, which also affects and may limit some DIC settings such as subset size. Therefore, the resolution of the image can be considered a basic parameter that primarily affects strain calculations. In this concept, Reu et al. (15) investigated the effect of camera resolution on DIC analysis and found that the loss of resolution reduced the DIC's accuracy and increased displacement errors. Nwanoro et al. (14) digitally resized the image resolution and repeated the DIC analysis with both the original and digitally converted images and concluded that the low-resolution images produced

higher error regions. There are also some recent studies on the resolution of strain maps of cracks in cement-based materials, however, in these studies, the common parameter investigated is the subset size, which may also be affected by camera resolution (16, 17).

In this study, the original resolution of the images was taken into account to investigate the effect of resolution on the determination of mechanical parameters and crack properties of ECC. For this purpose, simultaneous images were obtained with two identical cameras with different resolutions on the same ECC specimens, and the DIC results were discussed comparatively.

## MATERIAL AND METHODS

CEM I 42.5R type cement and granulated blast furnace slag (GBFS) were used as powder materials in the production of the specimens. The physical, chemical, and mechanical properties of cement and GBFS are presented in Table 1. High-tenacity polypropylene fibers (HTPP) were used as reinforcement, and their physical and mechanical properties are given in Table 2. A superplasticizer is also added to the mixture to obtain proper workability and distribute the fibers over the entire mixture. Material mixing ratios are shown in Table 3.

**Table 1.** Chemical, physical and mechanical properties of Portland cement and ground granulated blast furnace slag (GBFS).

| | | Portland Cement | GBFS |
|---|---|---|---|
| Chemical Composition (%) | SiO2 | 18.46 | 39.98 |
| | Al2O3 | 4.18 | 11.06 |
| | Fe2O3 | 3.17 | 0.77 |
| | CaO | 64.28 | 32.95 |
| | MgO | 1.27 | 10.26 |
| | Na2O | 0.50 | N/A* |
| | K2O | 0.84 | N/A |
| | SO3 | 3.14 | 0.34 |
| | Loss on Ignition | 3.60 | 2.34 |
| | Cl- | 0.006 | 0.0075 |
| | Free CaO | 1.80 | N/A |
| | Specific weight | 3.10 | 2.87 |
| | Blaine surface area (m²/kg) | 305 | 550 |
| | Compressive Strength (MPa) (at 2/7/28 days) | 28.5 / 43.0 / 54.3 | N/A |
| | Pozzolanic Activity Index (%) | N/A | 90 |

**Table 2.** Physical and mechanical properties of HTPP fibers

| | |
|---|---|
| Specific weight | 0.91 |
| Length (mm) | 10 |
| Diameter (mm) | 0.012 |
| Modulus of Elasticity (GPa) | 6 |
| Tensile Strength (MPa) | 850 |
| Elongation at Rupture | 21% |

**Table 3.** Mixture proportions of specimens (kg/m³)

| | |
|---|---|
| Cement | 390 |
| Granulated Blast Furnace Slag | 975 |
| Water | 507 |
| Superplasticizer | 1.6 |
| Fiber | 18 |

**Figure 1.** Pattern application to the specimens

In the production process, the powder materials are added to the mixer and then mixed as a dry mixture. The mixing process was continued by adding water and super-plasticizer to the mixture. Finally, HTPP fibers were added to the matrix, and it was manually checked whether the fibers were homogeneously distributed throughout the entire matrix without any agglomeration. Three bone-shaped tensile specimens were taken from the fresh mixture to the mold and kept in the mold for 1 day. The specimens were removed from the mold and cured in water for 28 days, and then left to dry in the air for 1 day. The patterning process was applied to the air-dried specimens to perform analyses with DIC. The specimens were first painted with white paint, and then a speckle pattern was applied to the specimen surfaces by using a stamp with a pattern generated by speckle generator software from Correlated Solutions (Fig. 1).

The tensile test setup with an integrated DIC system is shown in Fig. 2. A Shimadzu brand tensile device with a capacity of 50 kN was used in the tensile tests. After the bone-shaped specimens were placed in the jaws, extensometers (LVDTs) were placed at the four corners of the specimen with the help of a frame (Fig. 2a). A ring-shaped LED lighting system is placed just in front of the specimen to provide uniform illumination. Two Canon EOS 750D model DSLR cameras with 55-250 mm lenses of the same specification were used to take images from the midpoint of the ring LED during the experiment (Fig. 2b). The purpose of using two
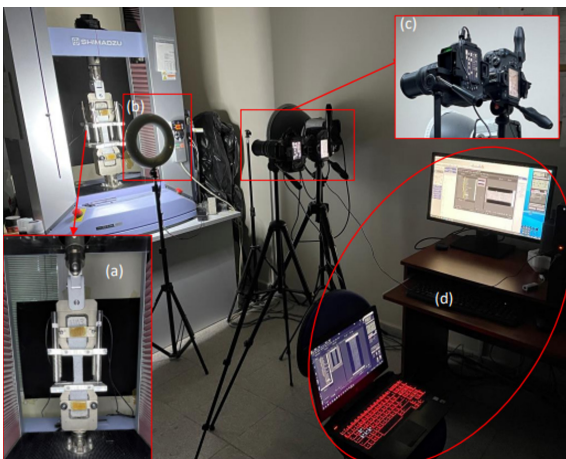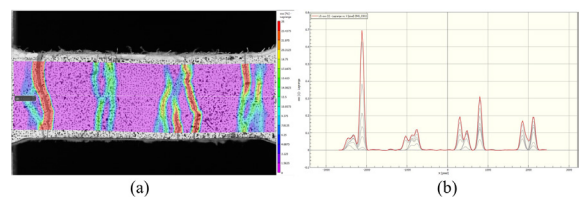
cameras is to obtain images from the same specimen but with two different resolutions to make comparisons accurately (Fig. 2c). The cameras were connected to two different data acquisition and analysis computers (Fig. 2d). During the tests, images were taken every 5 seconds using the remote management software of the cameras. The main camera settings have been determined as 24.2 MP resolution, 2 seconds of exposure time, F/20 aperture, and an ISO value of 100, taking into account previous experiences. Only the resolution of the auxiliary camera is decreased to 0.3 MP; other settings are kept constant.

First, the pattern intensities of the specimens (the number of black-painted pixels/total surface area in pixels), the number of spots in the pattern, and grayscale color histograms were determined via Matlab from the reference images taken at the beginning of the tests. In the tensile tests, an extensometer (LVDT) controlled loading procedure was applied with a loading rate of 0.5 mm/min. The tensile stress values were calculated by dividing the load values recorded during the test, by the cross-sectional area of the specimens ($\sigma_t$). The elongation values were recorded from the four LVDTs, and the average of these values was divided by the initial length of the specimen, and the unit strain values ($\varepsilon_{LVDT}$) of each specimen were calculated.

Vic-2D software was used to analyze the images taken during the experiments. The software offers the user a subset size that it deems appropriate according to the pattern quality of the area of interest (AOI) selected at the initial stage. The step size for the analysis was selected as 1/5 of the subset size as recommended by Tambusay et al. (16). Before starting the analysis, the resolution per pixel was measured and recorded via the software, and analysis was started. After the analyses were completed, the unit strain ($\varepsilon_{DIC}$) and local deformation values on the specimens were recorded with a virtual extensometer placed in the middle of each specimen (Fig. 3a).

Local deformations obtained from the virtual extensometer drawn from the middle of the specimen were used to calculate the crack number and width in accordance with Ohno and Li (11). Each peak on the local deformation curve was determined as a crack, and the area under this peak was calculated and characterized as the width of this crack (Fig. 3b).



**Figure 2.** a) Tensile specimens framed by 4 LVDTs, b) Ring LED lighting system, c) Two DSLR cameras, d) Data acquisition and analysis computers



**Figure 3.** a) Virtual extensometer placed to the middle of specimen, b) Obtaining local deformation data

By using the obtained data, stress-strain graphs of each specimen are drawn for both LVDT ($\sigma_t$-$\varepsilon_{LVDT}$) and DIC results ($\sigma_t$-$\varepsilon_{DIC}$) (Fig. 4). Peak stress values are determined ($\sigma_{t,max}$) and corresponding strain values are determined as strain capacities ($\varepsilon_{max,LVDT}$ and $\varepsilon_{max,DIC}$). The area under each curve up to strain capacity is also calculated and specified as peak ductility (PD). The difference between $\sigma_t$-$\varepsilon_{LVDT}$ and $\sigma_t$-$\varepsilon_{DIC}$ curves was calculated by subtracting the $\varepsilon_{DIC}$ value corresponding to each $\varepsilon_{LVDT}$ and taking its absolute value (Equation 1). All obtained values were summed up and expressed as the cumulative error ($\varepsilon_{acc}$) term (Equation 2). This term is important for interpreting the conformity of the strain values obtained by the traditional measurement method with the virtual extensometer and the amount of overlapping of the curves. However, the strain capacity of specimens may be different. Due to that, by dividing the $\varepsilon_{acc}$ by the ultimate strain ($\varepsilon_u$) obtained after softening, the strain error per unit strain is calculated and defined as the corrected cumulative error ($\varepsilon'_{acc}$) for a more accurate comparison.

$$\Delta\varepsilon_i = \left| \varepsilon_{LVDT,i} - \varepsilon_{DIC,i} \right| \tag{1}$$

$$\varepsilon_{acc} = \sum_0^i \Delta\varepsilon_i \tag{2}$$

$$\varepsilon'_{acc} = \frac{\sum_0^i \Delta\varepsilon_i}{\varepsilon_u} \tag{3}$$

According to Zhou et al. (18), the strain of the matrix contributes little to the overall strain of the ECC since the ECC deforms several hundred times more than the matrix forming the composite. Therefore, the overall deformation of the ECC can be considered to be related only to the crack opening, and the average crack width can be calculated by dividing the measured tensile deformation at the σt by the number of cracks (Equation 3):

$$w = \frac{\Delta l}{n} \tag{4}$$

where w: average crack width, $\Delta l$: the amount of axial elongation at $\sigma_{t,max}$, n: number of cracks visually counted from the surface of the specimen. Note that this method



**Figure 4.** Stress-strain curves and determination of tensile parameters

is only used for the $\sigma_{t,max}$ value in the literature since it is known that the number of cracks obtained as a result of mechanical tests does not increase after this value. Within the scope of the paper, the number of cracks was determined by counting from the middle region of the specimen, where the virtual extensometer was placed on the images via visual observations, and crack properties were discussed with DIC results at $\sigma_{t,max}$.

## RESULTS AND DISCUSSION

### Speckle Patterns

The averages of pattern intensities and the number of spots in the patterns were determined via Matlab and shown in Fig. 5. The pattern intensity of the images was 59.02% for the low-resolution images and 45.56% for the high-resolution images, respectively. However, the determined number of spots was 1725 on average for the low-resolution images. In the case of the high-resolution, this number increased by 538% and was counted as 11007 on average.

To further investigate these situations, closer image parts taken from Specimen 1 are presented in Fig. 6 and Fig. 7. Since the number of pixels corresponding to the same area of interest is increased, the sensitivity to catch details in the images is decreased, which causes the missed reflections in the pattern and decreased contrast (Fig. 6). Therefore, the pattern intensities were decreased in the high-resolution images. In addition to that, there is clear evidence that some spots appeared to be unified due to low light reflection and resolution. This clearly shows that the high-resolution images ensure a high number of points and high contrast for correlation calculations in DIC, which probably makes the analysis more accurate.

### Mechanical Parameters

$\sigma_t$-$\varepsilon_{LVDT}$ and $\sigma_t$-$\varepsilon_{DIC}$ curves obtained with DIC at two different resolutions are presented in Fig. 8. When the stress-strain curves are examined, there are slight fluctuations between the curves. Therefore, to make a more suitable comparison, the mechanical parameters (the tensile stress, strain capacity, and accumulated error values) and strain errors obtained from the curves are compared in Fig. 9.

The tensile strengths obtained from the curves were quite similar for LVDT, low-resolution DIC, and high-resolution DIC (Fig. 9a). Only the $\varepsilon_{max}$ and peak ductility (PD) values obtained from the high-resolution DIC curves seemed to be slightly higher than the LVDT and the low-resolution DIC results (Fig. 9a). This situation indicates that
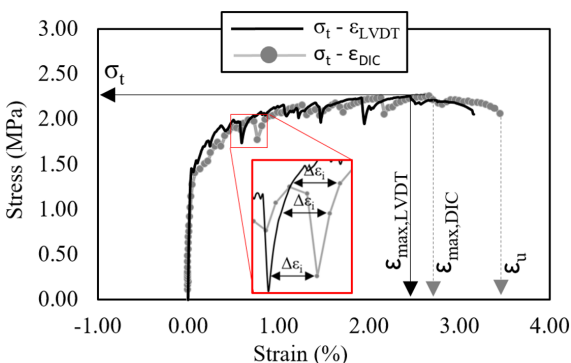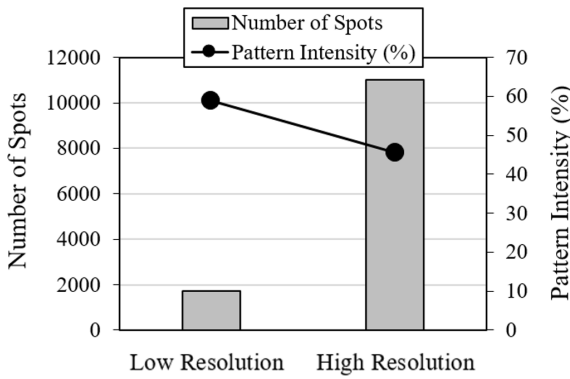
**Figure 5.** Comparison of pattern intensities and number of spots determined from the images by taking resolution into account.
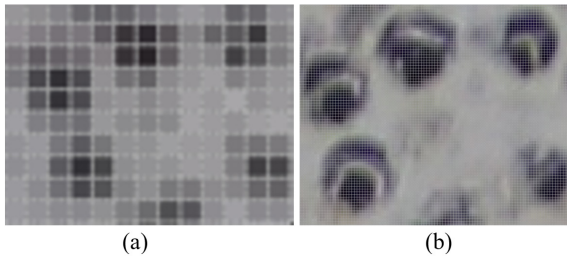


**Figure 6.** Effect of resolution to the pattern properties a) Low resolution, b) High resolution (representative part of the pattern taken from specimen 1)



**Figure 7.** Unified fields in the pattern a) Low resolution image, b) High resolution image (representative part of the pattern taken from specimen 1)

DIC has high potential to identify mechanical parameters regardless of the camera resolution. However, when Fig. 9b is taken into consideration, the strain errors obtained from the low-resolution DIC results were higher than the strain errors obtained from the high-resolution DIC results. When the high-resolution images were used in DIC analysis, the difference between the strain capacities ($\Delta\varepsilon_{max}$), accumulated strain errors ($\varepsilon_{acc}$), and corrected cumulative errors ($\varepsilon'_{acc}$) decreased by 50%, 18%, and 22%, respectively.

## Crack Properties

The effect of resolution on the detection of crack numbers and average crack width calculations are presented in Fig. 10. Average crack numbers can be followed on the first axis as dot graphs, and the average crack widths on the second axis as bar graphs. When the average number of cracks was compared, the number of cracks detected on the high-resolution DIC was almost double the number of cracks detected on the low-resolution DIC and closer to the crack number obtained from the visual observa-
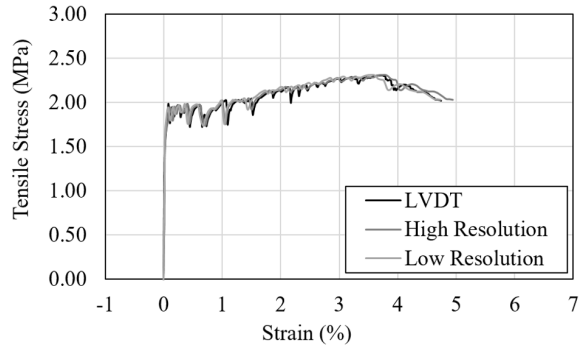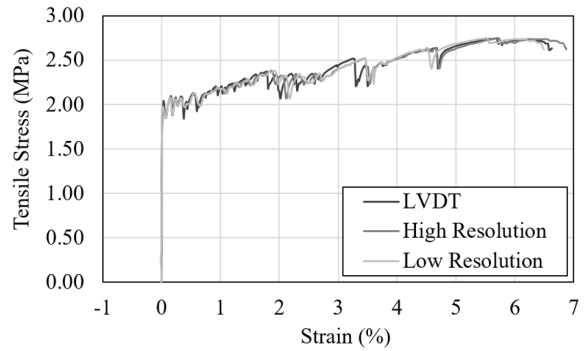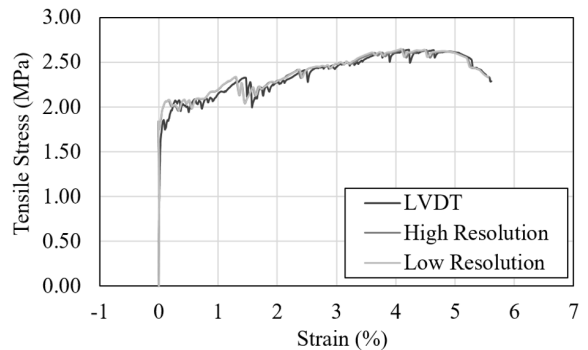


**Figure 8.** $\sigma_t$-$\varepsilon_{LVDT}$ and $\sigma_t$-$\varepsilon_{DIC}$ curves of specimens a) Specimen 1, b) Specimen 2, c) Specimen 3

tions on the specimens. When the average crack widths were examined, similar results were obtained. The average crack width calculated from the low-resolution DIC analysis was doubled compared to the average crack width calculated from the high-resolution DIC analysis. Also, the average crack width calculated from the high-resolution DIC analysis was remarkably close to the crack widths calculated by Equation 3.

The aforementioned crack properties only included the data corresponding to the $\sigma_{t,max}$ to compare the data obtained from DIC with the Equation 3, due to the limited use of the equation as explained in the previous sections. To further investigate and interpret the crack properties, crack propagations were investigated by using the local strain maps

## Mechanical Parameters



(a)

## Strain Errors



(b)
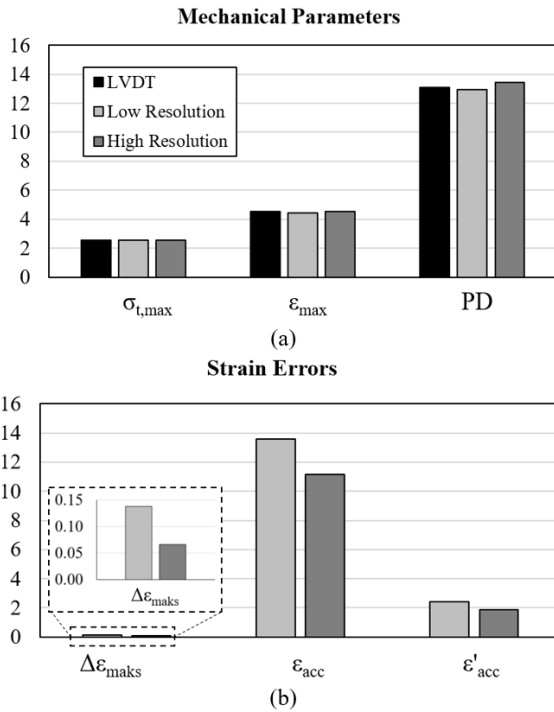
**Figure 9.** Comparison of a) Mechanical parameters, b) Strain errors
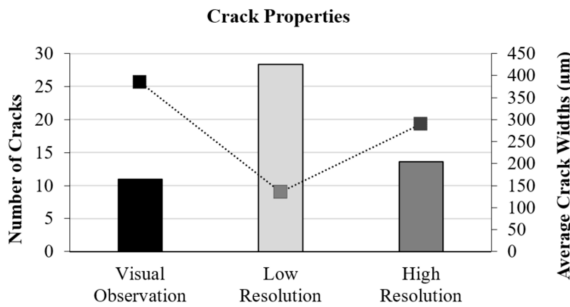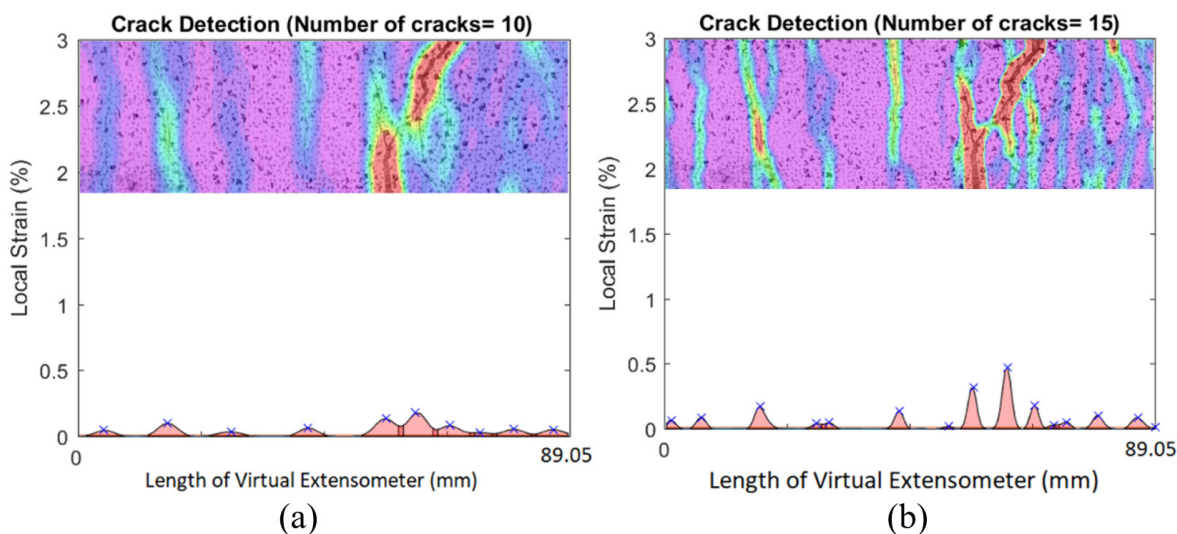
## Crack Properties



**Figure 10.** Crack properties at strain capacity

and crack properties obtained via DIC analysis from both low and high-resolution images (Fig. 11).

In Fig. 11, the crack propagation analysis of specimens was compared, starting at 0.5% strain and progressing through 1% strain intervals up to strain capacity. Average crack numbers can be followed as dot graphs on the first axis and the average crack widths on the second axis as bar graphs, as before. Light gray represents DIC results obtained from the low-resolution images, while dark gray represents the high-resolution images. The number of cracks determined from the high-resolution DIC is remarkably higher than the number of cracks determined from the low-resolution DIC. The average crack widths obtained from the high-resolution DIC are also remarkably lower than those obtained from the low-resolution DIC. It has been determined that this is due to the fact that cracks opened in close proximity to each other are considered a single crack due to the low-resolution, which decreased the detected number of cracks



(a)



(b)



(c)
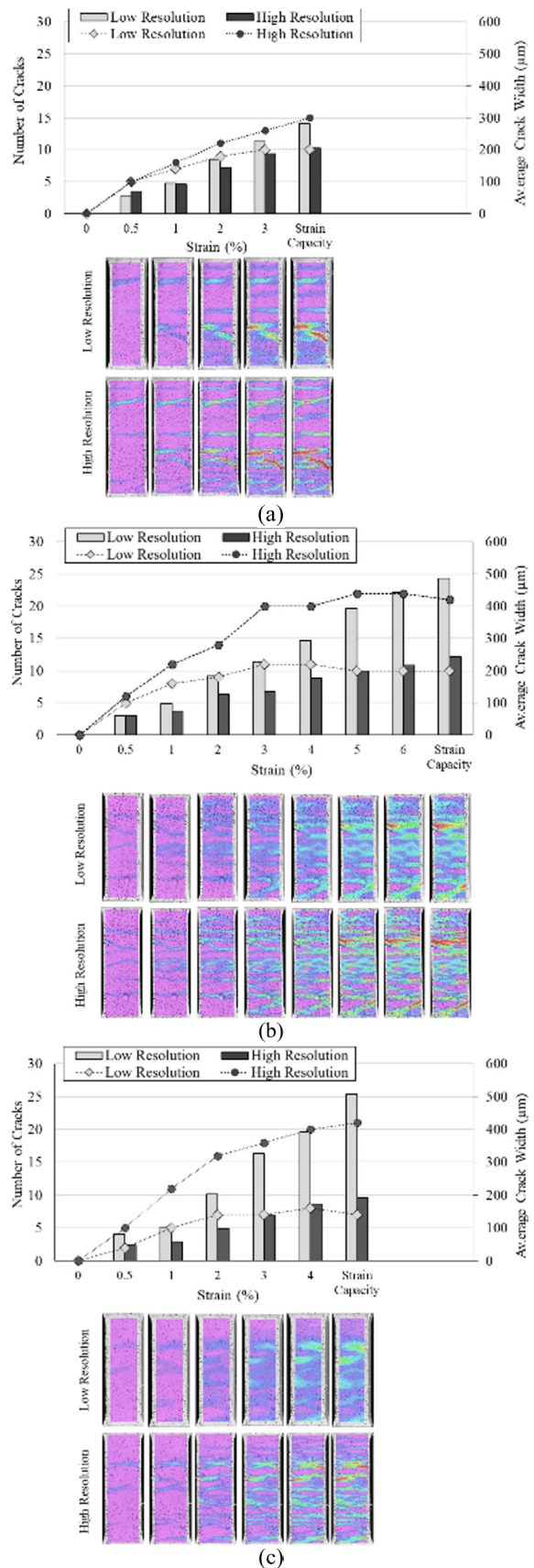
**Figure 11.** Crack propagation of specimens considering low and high resolution DIC analysis a) Specimen 1, b) Specimen 2, c) Specimen 3.

**Figure 12.** Effect of resolution to the crack properties a) Low resolution, b) High resolution (representative images taken from the Specimen 1)

and increased the calculated average crack widths (Fig. 12). This situation was recently reported by Tambusay et al. (16), and they concluded that increasing the subset size has the effect of introducing a blurring effect on crack maps of ECC and should be selected in relatively small sizes. Note that the subset size is directly affected by image resolution and using high-resolution images is one way to decrease the subset size. Therefore, the image resolution should be as high as possible for accurately tracking the crack propagation of ECC with relatively low subset sizes, as verified in Fig. 12.

One of the characteristic features of ECC is that the average crack width is stabilized at around 100 µm (19). This value is commonly used for poly-vinyl alcohol (PVA) fiber-reinforced ECC composites and is generally calculated by counting cracks and measuring their width with optical devices but in an unloaded state. By considering this, the crack widths in the range of 100-200 µm calculated under tensile loading conditions with DIC from the high-resolution images in this study can be considered reasonable (Fig. 11).

## CONCLUSION

In this study, the low and high-resolution images were captured simultaneously by two cameras during the tensile loading of the ECC, and DIC analysis was performed on the images. The effect of image resolution on the determination of mechanical parameters and the crack properties of ECC was investigated by comparing both DIC results and results from the traditional method. Mechanical parameters obtained through DIC analysis were found to be similar to traditional methods regardless of resolution, indicating that the DIC has a great opportunity for use in mechanical experiments. However, the high-

resolution images ensured a high number of points and relatively high contrast in the speckle patterns of specimens compared to the low-resolution images. This resulted in a low strain error when the high-resolution images were used in DIC analysis instead of the low-resolution images. Besides, both the detected number of cracks and the calculated crack widths were reasonable in the case of the high-resolution DIC analysis compared to the low-resolution DIC analysis. This situation was visually proven with the aid of local strain maps generated by DIC.

## ACKNOWLEDGEMENTS

## CONFLICT OF INTEREST

Authors approve that to the best of their knowledge, there is not any conflict of interest or common interest with an institution/organization or a person that may affect the review process of the paper.

## AUTHOR CONTRIBUTION

**Eren Gödek:** Research, Experiments, Analysis, Writing-Original draft preparation.
**Prof. Dr. Kamile Tosun Felekoğlu:** Supervisor, Writing, Reviewing and Editing, Project Administration.

# REFERENCES

1. Ding Y, Yu K, Li M. A review on high-strength engineered cementitious composites (HS-ECC): Design, mechanical property and structural application. Structures 2022;35:903-921. doi:10.1016/j.istruc.2021.10.036

2. Li VC. From micromechanics to structural engineering the design of cementitious composites for civil engineering applications. Doboku Gakkai Ronbunshu 1993;471:1-12. doi: 10.2208/jscej.1993.471_1

3. Kraft T, Riczo MJ, Chong A. Digital Image Correlation System Design, Verification and Analysis [internet]. Williams Honors College Honors Research Projects; 2022 [Date of access: 21.06.2023]. Erişim adresi: https://ideaexchange.uakron.edu/honors_research_projects/1555

4. Aghlara R, Tahir MM. Measurement of strain on concrete using an ordinary digital camera. Measurement 2018;126:398-404. doi:10.1016/j.measurement.2018.05.066

5. Alam SY, Loukili A, Grondin F. Monitoring size effect on crack opening in concrete by digital image correlation. European journal of environmental and civil engineering 2012;16(7):818-836. doi: 10.1080/19648189.2012.672211

6. Peters W, Ranson WF. Digital Imaging Techniques in Experimental Stress Analysis. Optical Engineering 1982;21(3):213427-213427. doi:10.1117/12.7972925

7. Sutton MA, Wolters WJ, Peters WH, Ranson WF, McNeil SR. Determination of Displacements using an Improved Digital Correlation Method. Image and Vision Computing 1983;3(1):133-139. doi:10.1016/0262-8856(83)90064-1

8. Choi S, Shah SP. Measurement of deformations on concrete subjected to compression using image correlation. Experimental mechanics 1997;37(3):307-313.

9. Sutton MA, Orteu JJ, Schreier H. Image correlation for shape, motion and deformation measurements: Basic concepts, theory and applications. Boston: Springer Science & Business Media; 2009.

10. Mahal M, Blanksvärd T, Täljsten B, Sas G. Using digital image correlation to evaluate fatigue behavior of strengthened reinforced concrete beams. Engineering Structures 2015;105:277-288. doi:10.1016/j.engstruct.2015.10.017

11. Ohno M, Li VC. A feasibility study of strain hardening fiber reinforced fly ash-based geopolymer composites. Construction and Building Materials 2014;57:163-168. doi:10.1016/j.conbuildmat.2014.02.005

12. Felekoglu B, Keskinates M. Multiple cracking analysis of HTPP-ECC by digital image correlation method. Computers and Concrete 2016;17(6):831-848.

13. Yu KQ, Yu JT, Dai JG, Lu ZD, Shah SP. Development of ultra-high performance engineered cementitious composites using polyethylene (PE) fibers. Construction and Building Materials 2018;158:217-227. doi:10.1016/j.conbuildmat.2017.10.040

14. Nwanoro K, Harrison P, Lennard F. Investigating the accuracy of digital image correlation in monitoring strain fields across historical tapestries. Strain 2022;58(1):e12401. doi:10.1111/str.12401

15. Reu PL, Sweatt W, Miller T, Fleming D. Camera system resolution and its influence on digital image correlation. Experimental Mechanics 2015;55(1):9-25. doi:10.1007/s11340-014-9886-y

16. Tambusay A, Suryanto B, Suprobo P. Digital image correlation for cement-based materials and structural concrete testing. Civil Engineering Dimension 2020;22(1):6-12. doi:10.9744/ced.22.1.6-12

17. Gehri N, Mata-Falcón J, Kaufmann W. Automated crack detection and measurement based on digital image correlation. Construction and Building Materials 2020;256:119383. doi:10.1016/j.conbuildmat.2020.119383

18. Zhou J, Qian S, Sierra Beltran MG, Ye G, van Breugel K, Li VC. Development of engineered cementitious composites with limestone powder and blast furnace slag. Materials and structures 2010;43(6):803-814. doi:10.1617/s11527-009-9549-0

19. Japan Society of Civil Engineers (JSCE). Recommendations for Design and Construction of High Performance Fiber Reinforced Cement Composites with Multiple Fine Cracks (HPFRCC). Concrete Engineering Series 82; 2008.